Structural design and experimental tests on a model of tensegrity greenhouse prototype

Giacomo Scarascia-Mugnozza,[1] Silvana Fuina,[1] Sergio Castellano[2]

[1]Department of Agricultural and Environmental Science, University of Bari Aldo Moro, Bari; [2]Department of Agriculture, Food, Natural resources and Engineering, University of Foggia, Italy

Abstract

The aim of this paper is the analysis, proposal and application of a structural tensegrity configuration for greenhouses supporting structures suitable for lightweight covering, based on principles of design coherence, material savings and building durability.

By means of the FEM software, Sofistik®, a tensegral greenhouse prototype was modelled and designed in accordance with EN 13031-1:2019.

In order to calibrate the results of the FEM analysis, experimental load tests and displacement measurements made with a tensegrity reduced scale model on a tensegrity reduced scale model, created at the Department laboratory of the University of Bari, were compared with the results of the calculation analysis. The displacements of the prototype selected nodes were detected by Target tracking Technology in two load configurations and a control transducer was positioned on the central structural node. The comparison among the displacements of the detected nodes with those resulting from the FEM software calculations, for two different load configurations, show average percentage errors of 7.1% and 12.55%. The results of the T test for the different load configuration point out that the two series of values experimentally detected and calculated by the software are not significantly different. Finally, results in terms of the structural steel weight and maximum stress of the tensegral structure were compared with those of commercial structures, both with vaulted roof and duo-pitched roof, of single span greenhouses having the same covered ground area of the greenhouse prototype. The proposed tensegrity greenhouse prototype showed a 9.6% and 35.2% reduction of the structural steel weight compared to the vaulted roof and to the duo-pitched roof greenhouse respectively.

Correspondence: Giacomo Scarascia-Mugnozza, Department of Agricultural and Environmental Science, University of Bari Aldo Moro, Via Amendola 165/A, 70126 Bari, Italy.
E-mail: giacomo.scarasciamugnozza@uniba.it

Key words: Experimental-loading tests; lightweight steel structures; standard EN 13031; structural analysis; tensegrity.

Acknowledgements: the authors would like to thank Massimiliano Nitti and Giovanni Attolico of the Italian National Council Research (CNR) Institute on Intelligent Systems for Automation of Bari, and Enrico Liano of the University of Bari for their support and contribution in the measuring system of the displacement detection.

Received for publication: 21 April 2021.
Accepted for publication: 27 May 2021.

Journal of Agricultural Engineering 2021; LII:1189
doi:10.4081/jae.2021.1189

Introduction

Greenhouse surface cultivation has increased worldwide over the last decades thanks to the high demand of vegetable and flower production (Giacomelli *et al.*, 2012). Despite the innovative cladding systems and materials (Stefani *et al.*, 2007; De Salvador *et al.*, 2008; Vox *et al.*, 2012) developed for both indoor climate equipment and cultivation techniques, the construction characteristics of greenhouse structures are still the traditional ones, *i.e.* duo-pitched roof greenhouses, vaulted roof greenhouses and tunnels. The aim of this research work is to develop with a prototype of a new supporting structure system for greenhouses, in order to obtain large free span in cultivation area, to enhance the behaviour of the structural construction material and to reduce the impact of both the structural weight and the structural shading on the cultivated internal area (Fuina *et al*., 2020). For this purpose, a structural tensegrity configuration suitable for lightweight cladding system buildings, like greenhouses, is proposed.

The term 'tensegrity' applied to innovative structures results from the merger of the words 'tensional' and 'integrity' and describes reticular structures formed by compressed elements 'immersed' in a continuous network of tense cables. Tensegrity technology allows the construction of structures suitable for covering large spans, thanks to the relatively small number of elements necessary for the structure, their level of prefabrication and their fast assembly (Nenadović, 2010). The mechanics of tensile systems compared to conventional structural systems has a number of advantages, because forces are naturally transferred along their shortest path to resist external loads, therefore only axial forces are generated. Indeed, tensile systems are able to vibrate and transfer loads, therefore they can absorb shocks and vibrations and, moreover, they can be extended indefinitely by assembling additional structures (Bansod *et al.*, 2014). Another fundamental characteristic is the lack of connection between the compressed elements, that produces a linear response of the nodes of the tensegral systems (Tibert and Pellegrino, 2003) and makes them interesting for the construction of 'intelligent' and 'foldable' structures. In fact, studies on the automated control of tensegrity structures are increasing (Sultan, 2014; Veuve *et al.*, 2016; Kan *et al.*, 2018). The possibility of creating many different shapes for tensegrity structures is a feature that makes this type of structure interesting from the point of view of engineering applications.

However, it may be a problem to identify the appropriate shape for these structures, since not all configurations of the structural elements can ensure system stability (Masic, 2004). The principle of tensegrity structures, despite being relatively recent, is becoming increasingly important also in the field of civil engineering and architecture. These tensile systems are configured thanks to their basic characteristics as structures capable of reacting to external and dynamic loads even by changing their configuration (Ali and Smith, 2010). This characteristic would therefore make the structures capable of responding to external actions, due for example to earthquakes, climatic actions like wind and snow, or thermal loads (d'Estree Sterk, 2003).

A particular type of tensegrity system is the 'cable dome' that has inspired this research work. Geiger and Levy successfully applied tensegrity dome systems to structures with large spans, for example in the 1985 Seoul Olympic Games gymnastics and fencing arenas (Figure 1), and in the 1994 Atlanta Olympic Games stadium (Motro, 2003). The tensegrity domes effectively combine a low structural mass with large spans, reaching 92 m for Seoul stadium and 227 m for Atlanta stadium.

According to Figure 1, we can identify two types of structural components: the compressed bars and the tensioned cables.

This research work is intended to propose a tensegrity structure suitable for the construction of greenhouses, that require large spans to increase the usable crop cultivation area, with thin structural sections to minimize the shading and a modular and easy-to-install structural element. It also envisages the possibility of using tensile structures for lightweight greenhouse facilities (Scarascia-Mugnozza and De Luca, 1990; Scarascia-Mugnozza, 2003). The most common types of greenhouses are often damaged due to a lack of a correct structural design to withstand the wind load and the snow load (Castellano *et al.*, 2004; Waaijenberg, 2004; Kong *et al.*, 2014; Briassoulis *et al.*, 2016; Dougka and Briassoulis, 2020). Therefore, the aim is to analyse different greenhouse structural systems able to adapt to the external load conditions.

Materials and methods

In order to determine an appropriate structural tensegrity configuration for greenhouses, a structural prototype of a tensegrity greenhouse with rectangular plan was designed in agreement with the EN 13031-1:2019 (European Committee for Standardization, 2019). In Italy this standard is not mandatory, therefore structural failures can occur, even for large greenhouse constructions, due to unfavourable very intense weather events.

For the purpose of validating the structural behaviour of the tensegrity prototype, the results of the FEM design software were calibrated with experimental tests carried out in the laboratory of the Department of Agricultural and Environmental Science of the University of Bari on a reduced scale (1:7) structural model. Finally, the results in terms of structural weight incidence per square meter of covered surface were compared with those obtained for commercial duo-pitched and vaulted greenhouses.

The design of the greenhouse supporting structure roof prototype was created starting from the simplest tensegrity configuration consisting of a truss made of two tension cables and a compressed strut (Figure 2A). In order to decrease the strut buckling length, in the second step two struts were inserted between the cables (Figure 2B). In the last step, a third strut and a secondary cable were added to split the system into multiple sections, thus creating a truss with three struts and three cables (Figure 2C).

The design hypothesis of the greenhouse prototype roof, derived from the truss scheme of Figure 2C, consists in two tensegrity trusses with a 15.86 m span, placed along the diagonals of the rectangular plan area of 9.50×12.70 m (Figure 2D). The trusses are hinged on the corners of the frame consisting in four columns joined with four beams. No lateral stability systems are foreseen for the main frame due to the fixed joint constraint at the base of the columns.

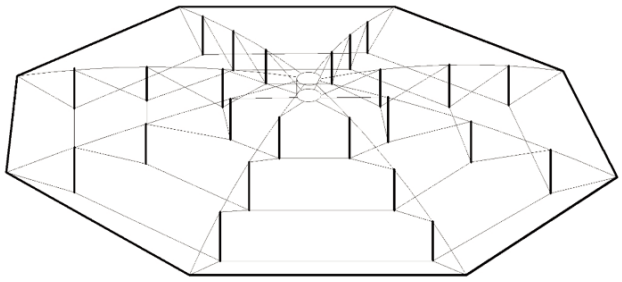

Figure 1. Structural scheme of the Seoul Olympic Games gymnastics and fencing arenas (92 m span). The compressed bars are shown in bold; the tense cables are shown with a thin line.

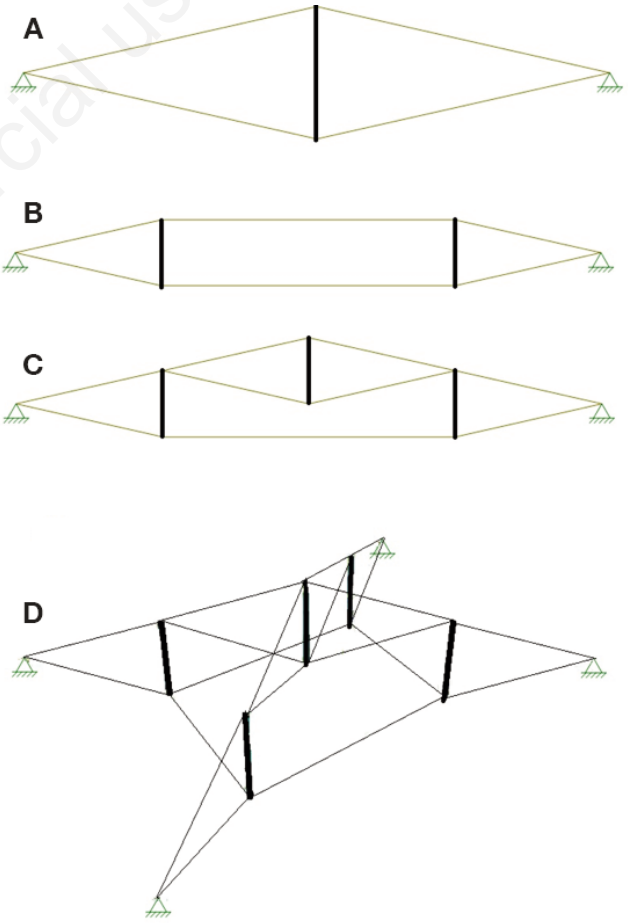

Figure 2. A) Tensegrity configuration with two cables and one strut. B) Tensegrity configuration with two cables and two struts. C) Tensegrity configuration with three cables and three struts. D) Structural scheme of the prototype tensegrity roof.

Theoretical models

The designed structure was modelled using a finite element software, SOFISTIK® 2014. The finite element method (FEM) used in the software is a displacement method and the mechanical behaviour is calculated with an energetic principle (minimization of the deformation energy). Struts and cable elements can transfer only axial forces. In the case of a non-linear analysis, the cable elements cannot support compression forces. Non-linear calculations make it possible to take into account the failure of particular elements, such as cables under compression. The non-linear material behaviour complies with the elastic-plastic law, which in turn complies with von Mises principle and includes hardening.

The designed prototype structural module has the following geometrical characteristics (Figure 3): rectangular plan with dimensions of 9.50×12.70 m and covered area of about 120 m^2, a gutter height of 3.50 m and a ridge height of 5.40 m, the slope of the two roof pitches with respect to the horizontal plane of 18° and 22°. Cables are 6×7 steel core wire ropes of stainless steel AISI 316, with a diameter of 14 mm and a tensile strength 1470 N/mm^2. Struts have a hollow circular section in S235 steel with a diameter of 44.5 mm and a thickness of 2.9 mm. As to the lower frame of the structure, columns are in S235 steel with a hollow circular section and have a 139 mm diameter and a 5 mm thickness. The 12.7 m-long beams are in S235 steel with a hollow circular section and have a 159 mm diameter and a 6 mm thickness, while the 9.5 m-long beams have a 152 mm diameter and a 3 mm thickness.

The structural self-weight of the designed tensegrity greenhouse was then compared with the two widespread commercial greenhouse structures, a duo-pitched roof greenhouse and a vaulted roof greenhouse in the single span configuration, with the same horizontal cultivation area of 120 m^2, and the same gutter height of 3.5 m.

The vaulted roof greenhouse (Figure 3) had the following structural features: ridge height of 5.9 m, columns with a IPE 120 section, roof arch having a hollow circular section with a 65 mm diameter and a 4 mm thickness, support elements having a hollow circular section with a 30 mm diameter and a 2 mm thickness. In the duo-pitched roof greenhouse (Figure 3), the ridge height was 5.9 m and the structural roofing elements had hollow rectangular sections of 80×50 mm and a 6 mm thickness, columns had a IPE120 section, the support elements had a hollow square section of 30×30 mm diameter and a 3 mm thickness. All structural elements of both the duo-pitched roof and the vaulted roof greenhouse were designed in S235 steel. An elastic modulus of 210 GPa was used for the calculation of all steel structures. Only for the cables a modulus of elasticity equal to 195 GPa was considered. All structural sections of the three types of greenhouses were designed by optimizing each structural element subject to the stress produced by the same design loading condition, using commercial steel sections. In order to proceed whit a correct structural comparison, accessory systems such as ventilation openings and roofing material fixing frames were not considered.

Calculation criteria

The design of the structural prototype of the tensegrity greenhouse (Figure 3) and the construction of the reduced scale structural model (Figure 4) were implemented by means of the EN 13031-1 (European Committee for Standardization, 2019).

The loads acting on the structure were determined based on the geographical location of the hypothesized structure according to the Italian Technical standards for Constructions: zone III for snow actions, zone III for wind actions and an elevation less than 200 m above sea level (Ministero delle Infrastrutture e dei Trasporti, 2018).

On the basis of this EN, we considered a minimum design working life for the structure of 15 years and a greenhouse type class B15, because Class B refers to greenhouses in which the cladding system can tolerate frame displacements resulting from the design actions. Therefore, with reference to the EN, we assumed 15 years as the minimum reference period for determining the characteristic values of the variable actions.

The characteristic values of the actions, referred to a return period of 50 years according to the Italian Technical standards for Constructions (Ministero delle Infrastrutture e dei Trasporti, 2018), were reduced to a return period of 15 years through the adjustment factors indicated in the EN: f_w(n) for wind loads and f_s(n) for snow loads (Table 1). These loading characteristic values of the actions were taken into account as distributed loads for the FEM model.

Regarding the calculation of the permanent actions on the greenhouse structures, we considered a covering material in single plastic film sheet of negligible weight.

The most severe combination of design values of the actions that may occur simultaneously was the load combination on the structures explained as combination a1) in the EN 13031-1, where the wind action is the leading variable action:

$$a1)\ \gamma_{G1}\, G_{k1} + \gamma_{G2}\, G_{k2} + \gamma_{Q1}\, Q_{k1} + \psi_{Q2}\, \gamma_{Q2}\, Q_{k2} + \psi_{Q3}\, \gamma_{Q3}\, Q_{k3} \quad (1)$$

Table 1 shows the design values used for the a1) combination of actions.

Experimental tests

Load tests were carried out on a reduced scale model 1:7 of the

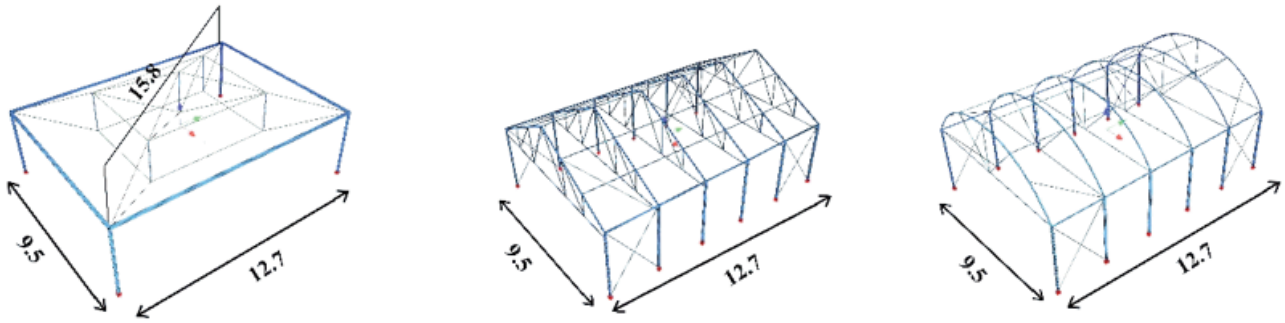

Figure 3. Tensegrity greenhouse prototype compared to commercial duo-pitched and vaulted roof greenhouses structures.

tensegrity greenhouse designed and built in the DISAAT laboratory of the University of Bari. In order to calibrate the structural analysis results, a comparison was made between the measured displacements of the experimental loaded nodes with the calculated displacements of the same nodes obtained by means of the FEM software Sofistik®. The geometrical characteristics of the reduced scale 1:7 model were the following: rectangular plan of 1.35×1.80 m, gutter height of 0.50 m, covered area of 2.43 m^2. The model was built with an AISI 316 stainless steel wire rope, with central tensioner, using 133 wires with a 5 mm diameter, construction of 6×19 M WSC, and strength of 1470 N/mm^2. The struts were made of AISI 316 steel with a circular hollow section with a 20 mm diameter and a 2 mm thickness. The pillars and beams of the structure lower frame were built and welded together in S355 steel with

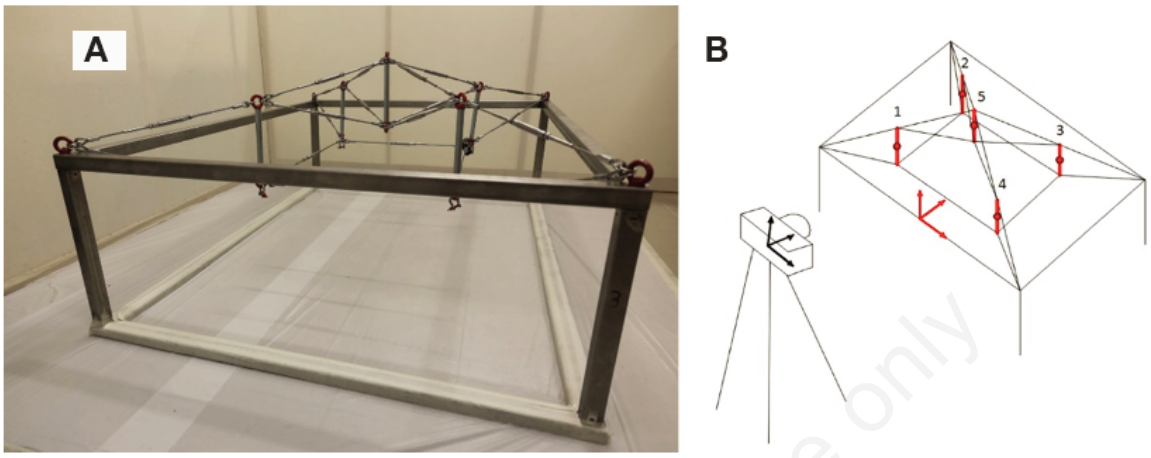

Figure 4. A) Reduced scale structural model prototype built at the Department laboratory of the University of Bari. B) Target tracking technology scheme of the selected loaded nodes of the structural prototype for the displacements analysis.

Table 1. Design values of actions and coefficients for the load analysis for the a1) combination of actions.

G_{k1}	Characteristic value of the permanent actions (self-weight of structural element)
γ_{G1}	Partial factor $\gamma_{G1} = K_{Fi,G1}\,\gamma_{F,G1,CC2}$ =9.0×1.3=1.17*
$\gamma_{F,G1,CC2}$	Partial factor of permanent actions for the reference consequence class CC2, according to Italian Technical standards
$K_{Fi,G1}$	Consequence factor for permanent actions depending from design working life
Q_{k1}	Characteristic value of the wind actions $Q_{k1} = f_w(n)\,q_{wind}\,c_p$
$f_w(n)$	Adjustment factor for wind load =0.86
q_{wind}	Kinetic pressure value of wind actions according to Italian Technical standards (zone III) =0.45 kN/m^2
c_p	Pressure coefficients for duo-pitched roof and vaulted roof structures defined respectively in the EN annexes B.2.2 and B.2.3. Pressure coefficients for the tensegrity roof shape are defined according to Italian Technical standards
G_{k2}	Characteristic value of the permanently present installation actions
γ_{G2}	Partial factor γ_{G2} =1.35
Q_{k2}	Characteristic value of the snow actions $Q_{k2} = f_s(n)s_{i,n,t} = f_s(n)\,\mu_i\,c_t\,s_{k,n}$
$f_s(n)$	Adjustment factor for snow load =0.63
μ_i	Shape coefficient =0.8
c_t	Thermal coefficient =1.0
$s_{k,n}$	Reference value of snow load on the ground according to Italian Technical standards (zone III) =0.60 kN/m^2
γ_{Q2}	Partial factor γ_{Q2} =1.35
ψ_{Qk2}	Combination coefficient for snow action ψ_{Qk2} =0.50 according to Italian Technical standards
Q_{k3}	Characteristic value of the crop actions for tomatoes or cucumber crops =0.20 kN/m^2
γ_{Q3}	Partial factor γ_{Q3} =1.35
ψ_{Qk3}	Combination coefficient for crop action ψ_{Qk3} =1.0 value is defined in the EN

*In order to show the calculation of the partial factor, only the example of the calculation of the partial factor γ_{G1} for permanent actions were reported.

hollow square profiles 40×40 mm and a 3 mm thickness. The nodes between cables and struts were assembled using M8 lifting eyebolts. The hooking of the cables to the eyebolts was made using stainless steel shackles with a pin diameter of 5 mm (Figure 4).

Four concentrated loads were progressively applied in four steps of 0.1 kN each to nodes 1, 2, 3 and 4 (Figure 4B) of the modelled structure in order to simulate a real load combination on the reduced scale model. Indeed, if the sum equal to 1.60 kN of the four final concentrated loads of 0.4 kN each is spread over the surface area of 2.43 m^2, it would correspond to a uniformly distributed load of 0.66 kN/m^2. In fact, with reference to the design values of actions in accordance with both the Italian Technical standards for zone III and the EN, the characteristic value of the snow actions is 0.60×0.80×0.63=0.30 kN/m^2, the characteristic value of the crop actions is 0.20 kN/m^2 and the characteristic value of permanently present installation actions is 0.13 kN/m^2, for a total roof uniformly distributed load of 0.63 kN/m^2.

During the loading tests each single concentrated load was applied hanging 4 modules of 0.1 kN to the eyebolts of nodes 1, 2, 3 and 4, corresponding to 4 struts (Figure 4A and B), in order to get an appropriate load progressiveness.

Two-load experimental configurations were implemented: i) the symmetrical load configuration 'A' when the four nodes 1, 2, 3 and 4 were simultaneously loaded with modules of 0.1 kN progressively applied and increasing up to 0.4 kN; ii) the asymmetrical load configuration 'B' when only the nodes 1 and 2 were simultaneously loaded with modules of 0.1 kN progressively applied and increasing up to 0.4 kN.

We repeated both the load experimental test configurations A and B 5 times. The node displacements were measured and gathered for each application of the 0.1 kN symmetrically and asymmetrically concentrated load.

During both loading test configurations A and B, a pretension of 36 N/mm^2 was applied to every cable of the experimental structure by means of the tensioner.

The nodal displacements of the selected points of the reduced scale model, the five nodes from n. 1 to n. 5 (Figure 4B), were detected by means of the digital image correlation (DIC) and Target tracking technology, which are methods for non-contact displacement monitoring in digital image processing (DIP). The position of a specific target in each frame of the image was detected setting a target board on the monitored point. The measurement of the single point displacement was evaluated by the target board displacement after processing the sampled image. The target board for sampling was designed with a checkerboard geometric pattern. Through a code written in C ++ ®, the positions of the centre of each target were correlated starting from the reference system of the camera (in black) with the positions in the chosen reference system (in red) (Figure 4B). The technology was used for structural monitoring (Franco *et al.*, 2017; Ngeljaratan & Moustafa, 2020).

Finally, with the aim of verifying the accuracy of the vertical displacements detected by the Target tracking technology, a transducer with a precision of 0.1 mm was positioned only at node n.5 and the related measurements were gathered during the experimental tests.

Results and discussion

The obtained results concerning both the symmetrical and the asymmetrical configuration experimental loading tests, the calculation design of the tensegrity greenhouse prototype and of the corresponding commercial production single span greenhouses were analysed and compared. By means of the results of the node displacements, gathered during the experimental load tests, it was possible to calibrate the calculation model of the tensegrity greenhouse.

Moreover, the FEM software calculations of the structural weight, the maximum stress and the maximum displacements at the eaves height of the tensegrity greenhouse were compared and analysed with the corresponding results obtained for the commercial greenhouse structures with the aim to evaluate the alternative use of tensegrities for greenhouse structures.

Calibration of the model

Figure 5 shows the average values of node n. 5 displacements, for the reduced scale structural model tensegrity prototype, detected by means of the Target tracking and the control Transducer technology, during the symmetrical and asymmetrical configuration experimental loading tests, compared with the corresponding displacements calculated by means of the FEM software. Displacements were measured along the vertical direction (z of the reference system), assuming the zero dimension in the undeformed unloaded configuration for each node. Results have positive values in case of downward displacements and negative values in case of upward displacements.

The results of the transducer system and software-calculated curves of node n. 5 displacements showed the same trend for the symmetric and asymmetric load configuration A and B, while the results of Target tracking and software-calculated curves showed the same trend for the symmetric load configuration A (Figure 5).

Target tracking and software-calculated curves diverge only for lightweight loading conditions in the asymmetric load configuration B, for very small software-calculated displacements of node n. 5 (Figure 5).

Tables 2 and 3 show the results of the vertical nodal displacements of the experimental reduced scale model, according to the different load configurations A and B, measured by means of two different methods, Target tracking technology (TA for the nodes n.1, 2, 3, 4, 5) and Transducer system (TR for the node n. 5). For the comparative analysis between the experimental results and the software-calculated ones, both percentage errors and T tests were considered.

For the symmetric load configuration A (Table 2), the software-calculated displacements of nodes n. 1, 2, 3 and 4 are shown together in the second column, because they are identical values.

Instead, for the asymmetric load configuration B (Table 3), the software-calculated displacements of nodes n.1 and n.2 are shown together in the second column, because they are identical values. The same applies to nodes n.3 and n.4 shown in the seventh column.

Under the symmetric load configuration A (Table 2) the maximum percentage error among the displacement values detected by the target and the software was 24.0%, and the average percentage error was 7.1%, while the maximum and average percentage errors among the displacement values detected by the transducer and the calculated ones were 8.0% and 2.6% respectively.

Under the asymmetric load configuration B (Table 3) the maximum percentage error among the displacement values detected by the target and the software was 50.6%, and the average percentage error was 12.55%, while the maximum and the average percentage errors among the displacement values detected by the transducer and the calculated ones were 9.8% and 5.7% respectively. For this loading configuration, it can be pointed out that the maximum percentage errors were gathered for nodes n. 5, 50.6% error, and node n. 3, 33.8% error, both for the Target tracking measurement technology. Moreover, node n. 3 showed the maximum error (24.0%)

also for the load configuration A, and the errors happened for all the mentioned cases during the first loading application step of the 100 N concentrated load. Even the Transducer system method showed the maximum percentage errors for node n. 5, much lower than the Target errors, during the first 100 N loading application step for both load configurations A, 8.0% error, and B, 9.8% error.

The remarkable deviation of the measured target values of node n.5 in the asymmetric load configuration B for the first loading step (100 N) may be caused by the very small values of the software-calculated displacements: only 0.5 mm (Figure 5 and Table 3). Probably the settlements of the structural elements converging in the same top node of the reduced scale structure

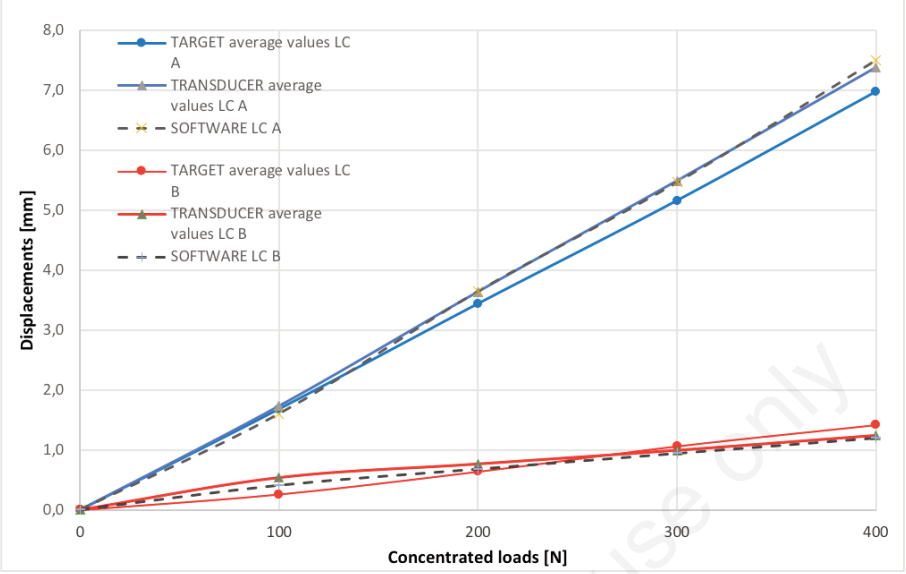

Figure 5. Average values of the measured vertical displacements of node n. 5 for the load configuration A (in blue) and for the load configuration B (in red) compared to the calculated vertical displacements (dashed line).

Table 2. Vertical displacements of nodes from n. 1 to n. 5 for the load configuration A.

		LOAD CONFIGURATION A												
		1		2		3		4		5				
Load [N]	SO [mm]	TA [mm]	ERR [%]	TA [mm]	ERR [%]	TA [mm]	ERR [%]	TA [mm]	ERR [%]	SO [mm]	TA [mm]	ERR TA-SO [%]	TR [mm]	ERR TR-SO [%]
0	0.0	0.0		0.0		0.0		0.0		0.0	0.0		0.0	
100	4.6	4.4 ± 1.5	3.1	4.4 ± 2,4	3.1	3.5 ± 1.0	24.0	4.1 ± 0.4	9.9	1.6	1.7 ± 0.3	4.9	1.7 ± 0.1	8.0
200	7.5	7.3 ± 0,6	2.6	6.1 ± 3.0	18.1	5.9 ± 0.7	21.7	7.0 ± 0.5	6.8	3.7	3.4 ± 0.3	5.7	3.6 ± 0.1	0.3
300	9.4	10.2 ± 0,8	9.3	8.1 ± 3.8	13.6	8.5 ± 0.4	9.6	9.5 ± 0.3	1.9	5.5	5.2 ± 0.4	5.5	5.5 ± 0.1	0.4
400	11.2	12.5 ± 0.7	11.9	10.2 ± 3.8	8.3	10.9 ± 0.5	2.6	12.3 ± 0.6	9.9	7.5	7.0 ± 0.4	7.0	7.3 ± 0.1	1.7

SO, displacements resulting from Software; TA, average value±standard deviation of displacements detected by Target Technology; TR, average±standard deviation of displacements detected by Transducer system; ERR TA-SO, percentage error between values detected by Target and software values; ERR TR-SO, percentage error between values detected by Transducer and software values.

Table 3. Vertical displacements of nodes from n. 1 to n. 5 for the load configuration B.

		LOAD CONFIGURATION B													
		1		2			3		4		5				
Load [N]	SO 1-2 [mm]	TA [mm]	ERR [%]	TA [mm]	ERR [%]	SO 3-4 [mm]	TA [mm]	ERR [%]	TA [mm]	ERR [%]	SO [mm]	TA [mm]	ERR TA-SO [%]	TR [mm]	ERR TR-SO [%]
0	0.0	0.0		0.0		0	0.0		0.0		0.0	0.0		0.0	
100	13.6	11.9 ± 1.2	12.6	10.3 ± 1.4	24.1	12.6	-8.3 ± 0.4	33.8	-10.5 ± 0.6	17.0	0.5	0.26 ± 0.3	50.6	0.6 ± 0.1	9.8
200	17.1	16.8 ± 1.2	2.1	15.3 ± 1.3	10.7	15.8	-13.7 ± 0.4	13.4	-16.2 ± 0.4	2.2	0.8	0.6 ± 0.2	15.0	0.8 ± 0.1	7.4
300	19.7	20.1 ± 1.1	1.9	18.8 ± 1.0	4.8	18.0	-17.6 ± 0.3	2.3	-20.4 ± 0.3	13.6	1.0	1.1 ± 0.2	4.9	1.0 ± 0.1	2.4
400	21.9	22.6 ± 1.0	3.4	21.4 ± 0.7	1.9	19.7	-20.8 ± 0.3	5.0	-23.6 ± 0.4	18.2	1.2	1.4 ± 0.2	13.6	1.3 ± 0.1	3.0

SO 1-2, displacements resulting from Software for nodes 1 and 2; SO 3-4, displacements resulting from Software for nodes 3 and 4; TA, average value±standard deviation of displacements detected by Target Technology; TR, average±standard deviation of displacements detected by Transducer system; ERR TA-SO, Percentage error between values detected by Target and software values. ERR TR-SO, percentage error between values detected by Transducer and software values.

occurred in asymmetric conditions, after the starting low loading conditions that caused almost zero displacements of node n. 5. Indeed, as the displacements data realigned for more severe load conditions (200-300-400 N), the values detected by the Target tracking technology were comparable with those detected by the Transducer system, and both showed a low percentage error (Table 2 and 3), when compared with the still small software-calculated values (0.8, 1.0 and 1.2 mm).

All the results confirmed that it is important to perform a verification by means of the Transducer system with a precision of 0.1 mm to check the accuracy of the vertical displacements experimental data detected by the Target tracking technology. Indeed, we can say that the Target tracking technology has poor precision in case of very small displacement values.

The root mean square error was calculated on the data collected by Target tracking in the load configurations A and B. The values obtained were normalized with respect to the maximum displacement value recorded in each test, obtaining normalized RMSE in both configurations equal to 8%.

Moreover, after a statistical analysis of the experimental results, the average of the values detected by Target Tracking measurement method for each node, according to the load configuration, was compared with the values obtained by the software-calculated displacements through a T test. The outcome of the T test for both load configuration A and B was 0.73, therefore we can say that the two series of values experimentally detected and calculated by the software are not significantly different.

The experimental results of the displacements on the loaded tensegrity scale model, obtained by means of two different measurement technologies, fitted well with the results of the calculation made by FEM software. Therefore, it is possible to state that the calculation software calibrated well for the proposed structural model of the tensegrity greenhouse prototype.

Structural design and comparison with commercial greenhouses

After having demonstrated the correct design methodology of the innovative prototype structure, it was possible to develop and verify the structural project of a tensegrity greenhouse, and make a comparison of the tensegrity greenhouse structure with the vaulted roof and duo-pitched roof commercial production single span greenhouse structures (Figure 3) with the same covered ground area. For this purpose the maximum displacement of the columns at the height of the eaves, the maximum displacement of the ridge of the roofs, the distribution of the bending moments, the maximum stresses and the weight of the steel structure per square meter of the three different structures under the same design loading con-

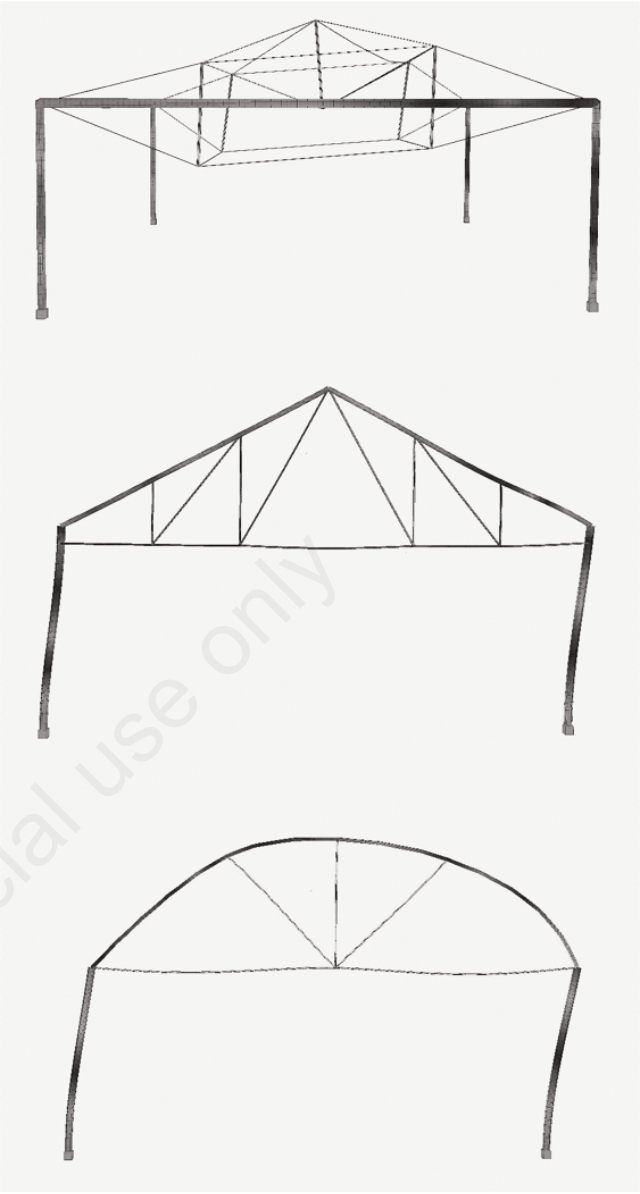

Figure 6. Deformed configuration of the greenhouses under the a1) combinations of actions. The deformation scale factor is equal to 1 for the tensegrity greenhouse and equal to 10 for duo-pitched and vaulted greenhouses.

Table 4. Structural steel weight per square meter, maximum vertical displacement of the roof ridge, maximum displacement of the columns at the eave height, maximum bending moment and normal stress of the most stressed columns of the different greenhouses under the same design loads of the combinations of actions a1).

	Tensegrity greenhouse	Duo pitched greenhouse	Vaulted roof greenhouse
Structural steel weight per square meter [N/m^2]	91.4	141.1	101.2
Max vertical displacement of the roof ridge [mm]	138.7	8.97	12.6
Max horizontal displacement of columns at the eave height [mm]	62.1	37.7	51.0
Max stress At the base of the columns	N=29.0 KN M=13.8 kNm	N=11.6 KN M=11.2 kNm	N=11.0 KN M=11.9 kNm

dition were computed, analysed and compared.

In order to develop and verify the supporting structures of the types of greenhouses considered, we applied the heaviest load condition among the combinations of actions recommended by the EN. The heaviest load condition we calculated on the analysed greenhouse structures was the combination of design actions classified by the EN as a1) and shown in Table 1.

Moving on to the full-scale software model of the tensegrity greenhouse the order of magnitude of the displacement of the columns at the gutter level was equal to 62.1 mm under the a1) combination of actions (Figure 6). With the same loading combination, the vaulted roof greenhouse and the duo-pitched greenhouse underwent a maximum displacement of columns at the gutter level equal to 51.0 mm and to 37.7 mm respectively (Table 4).

The most severe values of the bending moments occurred at the base of the columns for the tensegrity, the vaulted roof and the duo-pitched greenhouse structures (Figure 7A-C), while they occurred also on the compressed perimeter ring beams at the height of the eaves for the tensegrity structure in the rectangular ring plane.

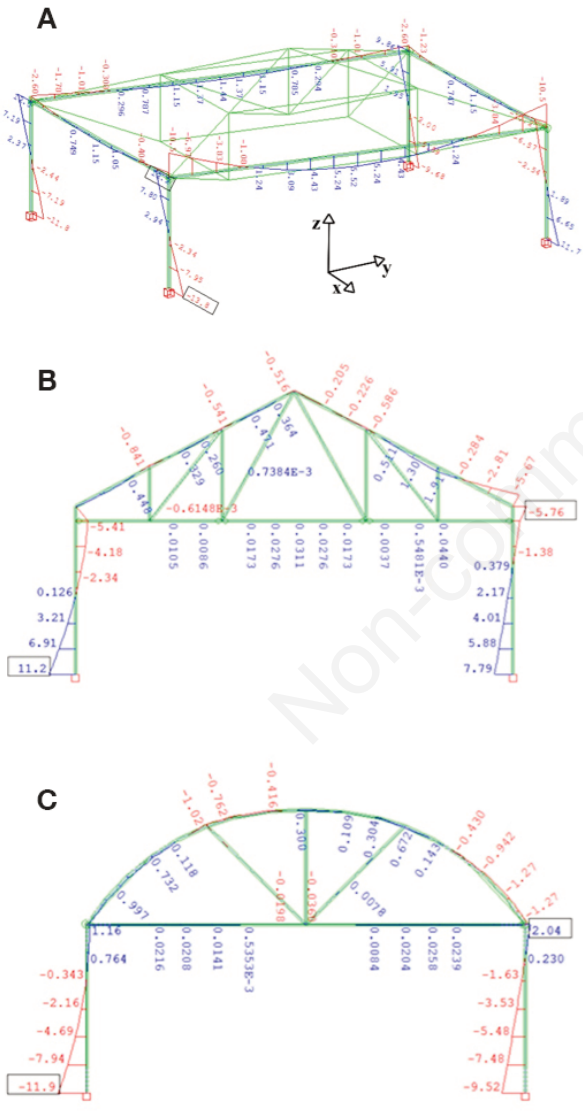

Figure 7. Bending moment (kNm), with respect to y-axis, of the calculated greenhouse structures under the a1) combination of actions: A) tensegrity greenhouse; B) duo-pitched greenhouse; C) vaulted roof greenhouse.

The outcomes of the bending moments and the normal stress distribution on the three analysed greenhouse structures showed a quite different structural behaviour of the tensegrity greenhouse compared to that of the traditional greenhouse structures. Indeed, the roofing system of traditional greenhouses could be assimilated to a truss girder in which structural elements are prevalently subject to compression or traction forces with low levels of bending moments. The planar behaviour of the frames of both the duo pitched and the vaulted roof greenhouses, having six columns on each sidewall, induced maximum bending moments only at the base of the columns. On the other hand, the spatial behaviour of the proposed tensegrity structure having two columns on each side of the perimeter wall gave the maximum bending moment (with respect to the z-axis in the x-y ring plane) on the perimeter ring beams subject to the combined bending and compression forces. In this case, cables and struts of the roofing system of the tensegrity structure were only subject to traction and compression forces respectively.

As regards to the maximum vertical displacement of the roof ridge, the tensegrity structure showed a greater displacement (138.7 mm) that occurred to the cables and struts portion of the structure and did not involve the deformation of the structural beams and columns unlike what happened in the compared greenhouses (Figure 6). The designed tensegrity structure had only 4 columns subject to stress and displacements in comparison to the 12 columns of the commercial greenhouse structures and, consequently, only 4 foundation plinths.

Table 4 shows the highest bending moments and the associated normal stress of the columns for the three structures and summarizes the main differences between the three structures. Comparing the overall structural steel weight per square meter of the greenhouse covered area, without considering the effect of the foundations, the tensegrity structure (93.7 N/m^2) is lighter than the traditional commercial steel greenhouse constructions (Table 4).

The tensegrity greenhouse, thanks to the cables and struts structural geometry of the roof, made it possible to achieve a reduction of the structural steel weight per square meter of 9.6% less than a vaulted roof greenhouse and of 35.2% less than a duo-pitched greenhouse. Therefore, also a lower structural shading (Fuina *et al.*, 2020) on the ground cultivation area can be obtained.

Conclusions

In this paper a prototype of a tensegrity greenhouse was designed in agreement with the EN 13031-1:2019 and the Italian national construction standards in order to propose innovative structures suitable for lightweight cladding system, large free span, reduction of the structural weight and the structural shading on the inside cultivation surface.

With the aim of validating the structural behaviour, the results of the FEM software calculation were calibrated with experimental tests carried out on a reduced scale model. Node displacements measurements, detected by means of the DIC and the Target tracking technology, under different load configurations, showed that the experimental data fit well with the results of the calculation made by FEM software.

The Root Mean Square Error, normalized RMSE and T test of the measurements data processing showed that there are no significant differences among experimental and calculation results.

Finally, the results in terms of structural weight incidence per square meter were compared with those obtained from the analysis of commercial greenhouses and made it possible to obtain a reduction in the structural steel weight per square meter by 9.6% compared to a vaulted roof greenhouse and by 35.2% compared to a duo-pitched greenhouse.

The structural behaviour of the tensegral greenhouse can represent an advantage, because the structural elements, cables and struts, which make up the roofing system, undergo significant displacements, but are also recoverable once the structure is unloaded, allow a saving of both structural steel and foundation and induce a lower structural shading on the ground cultivation area. Future research will deal with multi-span tensegrity greenhouses for large horticultural plants and with the design effects of the ventilation openings, covering material supporting systems and foundations.

References

Ali N.B.H., Smith I.F.C. 2010. Dynamic behavior and vibration control of a tensegrity structure. Int. J. Solids Struct. 47:1285-96.

Bansod D. Y., Nandanwar D., Burša, J. 2014. Overview of tensegrity - I : Basic structures. Engine. Mechan. 21:355-67.

Briassoulis D., Dougka G., Dimakogianni D., Vayas, I. 2016. Analysis of the collapse of a greenhouse with vaulted roof. Biosyst. Engine. 151:495-509.

Castellano S., Candura A., Scarascia-Mugnozza, G. 2004. Greenhouse structures SLS analysis: Experimental results and normative aspects. Acta Hortic. 691:701-8.

d'Estree Sterk T. 2003. Using actuated tensegrity structures to produce a responsive architecture. pp 84-93 in ACADIA22: Connecting Crossroads of Digital Discourse.

De Salvador F.R., Scarascia Mugnozza G., Vox G., Schettini E., Mastrorilli M., Bou Jaoudé M. 2008. Innovative photoselective and photoluminescent plastic films for protected cultivation. Acta Hortic. 801:115-21.

Dougka G., Briassoulis D. 2020. Load carrying capacity of greenhouse covering films under wind action: Optimising the supporting systems of greenhouse films. Biosyst. Engine. 192:199-214.

European Committee for Standardization 2019. EN 13031-1. Greenhouses: design and construction. Part 1: Greenhouses for commercial production. CEN, Brussels.

Franco J. M., Mayag B. M. Marulanda, J., Thomson, P. 2017. Static and dynamic displacement measurements of structural elements using low cost RGB-D cameras. Engine. Struct. 153:97-105.

Fuina S., Scarascia-Mugnozza G., Castellano S. 2020. Innovative tensile structures for protected crop facilities. Lecture Notes Civil Engine. 67:247-53.

Giacomelli G.A., Sase S., Cramer R., Hoogeboom J., MacKenzie A., Parbst K., Scarascia-Mugnozza G., Selina P., Sharp D.A., Voogt J.O., van Weel P.A., Mears D. 2012. Greenhouse production systems for people. Acta Hortic. 927:23-38.

Kan Z., Peng H., Chen B., Zhong, W. 2018. A sliding cable element of multibody dynamics with application to nonlinear dynamic deployment analysis of clustered tensegrity. Int. J. Solids Struct. 130-131:61-79.

Kong B. W., Quiao K., Yuan J. 2014. The investigation of long-span double-layer reticulated dome greenhouse's dynamic characteristics. pp 338-343 in International Conference on Mechanics and Materials Engineering.

Masic M. 2004. Design, optimization, and control of tensegrity structures. Doctoral dissertation, University of California, San Diego, CA, USA.

Ministero delle Infrastrutture e dei Trasporti. 2018. D.M. 17 gennaio 2018: Aggiornamento delle Norme tecniche per le costruzioni. Gazzetta Ufficiale della Repubblica Italiana. Istituto Poligrafico dello Stato, Roma, 52-60.

Motro R. 2003. Tensegrity: structural systems for the future. Kogan Page Science, London, UK.

Ngeljaratan L., & Moustafa M. A. 2020. Structural health monitoring and seismic response assessment of bridge structures using target-tracking digital image correlation. Engine. Struct. 213:110551.

Nenadović A. 2010. Development, characteristics and comparative structural analysis of tensegrity type cable domes. Spatium 22:57-66.

Scarascia-Mugnozza G., De Luca, V. 1990. La realizzazione di serre di grandi dimensioni con tipologie a tensostruttura. Riv. Ing. Agr. 21:106-16.

Scarascia-Mugnozza G. 2003. Strutture e tipologie nuove negli impianti serricoli. Colture Protette. 32:89-104.

Stefani L., Zanon M., Modesti M., Ugel E., Vox G., Schettini E. 2007, October. Reduction of the environmental impact of plastic films for greenhouse covering by using fluoropolymeric materials. In International Symposium on High Technology for Greenhouse System Management, Greensys2007, 801:131-8.

Sultan C. 2014. Tensegrity deployment using infinitesimal mechanisms. Int. J. Solids Struct. 51:3653-68.

Tibert A. G., Pellegrino S. 2003. Review of form-finding methods for tensegrity structures. Int. J. Space Struct. 18:209-23.

Veuve N., Dalil Safaei S., Smith, I. F. C. 2016. Active control for mid-span connection of a deployable tensegrity footbridge. Engine. Struct. 112:245-55.

Vox G., Scarascia-Mugnozza G., Schettini E., de Palma L., Tarricone L., Gentilesco G., Vitali M. 2012. Radiometric properties of plastic films for vineyard covering and their influence on vine physiology and production. Acta Hortic. 956:465-72.

Waaijenberg D. 2004. Design, construction and maintenance of greenhouse structures. Acta Hortic. 710:31-42.